Optical beams in saturable self-focusing media

Magnus Karlsson
Institute for Electromagnetic Field Theory, Chalmers University of Technology, S-412 96 Göteborg, Sweden
(Received 17 December 1991)

An approximate analytical analysis of two-dimensional optical beams propagating in saturable self-focusing media is carried out. In particular, the radial shape and the phase shift of the stationary self-trapped fundamental mode are investigated in detail. The dynamic variations of the beamwidth and the phase shift for nonstationary propagation are also analyzed. The predictions of the analytical model are compared with numerical results for stationary propagation and show good agreement.

PACS number(s): 42.65.Jx, 42.50.Rh

I. INTRODUCTION

Spatial solitons, i.e., optical beams that are self-trapped in space due to a balance between the Kerr nonlinearity and diffraction, have attracted considerable interest recently. Several theoretical investigations have been published [1–6], and spatial solitons have also been verified experimentally [7]. The physical background, i.e., the fact that the Kerr nonlinear refractive index can cause optical beams to self-focus and self-trap in space has been well known since the 1960s [8]. The formal equivalence between self-focusing in space and pulse compression in time was also established early [9], and under certain circumstances (anomalous dispersion and space-time symmetry), the comoving time coordinate can be treated as a transverse dimension [2,3]. In particular, Silberberg [2] has suggested the possibility of creating light bullets that are prevented from diffracting in space and dispersing in time by the Kerr nonlinearity.

However, it has been shown [2,3] that beams which are self-guided in more than one transverse dimension are unstable, and will either diffract away, or self-focus catastrophically, when perturbed. There are, however, several ways to get around this stability problem and to create stable, self-guided beams in two or more transverse dimensions. The most obvious way is to use a graded-index fiber, which prevents the power from diffracting away, thus opening a way to create stable beams, provided the beam power is below the self-focusing power. Above the self-focusing threshold, however, such beams will collapse (see Ref. [10]). A way of making self-guided beams stable above the self-focusing power is to prevent the catastrophic collapse by taking into account that the nonlinear refractive index saturates at high powers, as pointed out by Snyder *et al.* [4]. It should thus be of great interest to study saturable media in more detail, since they may provide a way to create stable solitons that are self-trapped in more than one transverse dimension.

The onset of saturation in the nonlinear refractive index was examined analytically very early by use of the paraxial-ray approximation [11,12]. Some numerical results were also published in the late 1960s [13,14]. Higher than third-order nonlinearities, i.e., nonlinearities with qualitative saturation behavior, were examined numerically by Piekara, Moore, and Feld [15]. The moment theory, which is an exact approach, was used to examine the mean-square radius of a self-trapped beam in a saturable nonlinear medium by Lam, Lippman, and Tappert [16,17]. Anderson and Bonnedal showed [18] that a variational approach gives results in exact agreement with the moment theory. The variational approach has also been used in a few recent studies on the subject [19,20]. In another recent numerical analysis by Chen [21] the self-trapped mode profiles were shown to depend on the self-trapped amplitudes, and one aim of the present work is to present an analytical derivation of these results.

In the subsequent analysis we will consider a refractive index n of the following form:

$$n^2=n_0^2+\frac{n_0 n_2|E|^2}{1+n_0 n_2/(n_{\rm sat}^2-n_0^2)|E|^2}\ , \tag{1.1}$$

where we have denoted the envelope of the electric field with E, the saturated index with $n_{\rm sat}$, and the nonlinear Kerr coefficient with n_2. This kind of saturable refractive index exists in various kinds of materials: dilute gases [13] and other ensembles of polarizable molecules [14], under certain conditions in plasmas [18,22], and also in acid glasses with high nonlinear coefficients [21]. The equation that governs the evolution of the electrical-field envelope in such media is the nonlinear Schrödinger (NLS) equation, modified to take saturation effects into account, i.e.,

$$\frac{1}{r}\frac{\partial}{\partial r}\left[r\frac{\partial\Psi}{\partial r}\right]-2ik\frac{\partial\Psi}{\partial z}+\frac{k^2|\Psi|^2\Psi}{1+\gamma^2|\Psi|^2}=0\ , \tag{1.2}$$

where we have introduced the normalized nonlinear amplitude $\Psi^2=(n_2/n_0)E^2$ and the saturation constant $\gamma^2=n_0^2/(n_{\rm sat}^2-n_0^2)$. The radial and longitudinal coordinates are denoted r and z, respectively, and k is the linear wave number. Note also that we are considering two transverse dimensions in Eq. (1.2) and that they can be either both in space, or, if we have space-time symmetry, one in space and one in time; cf. Refs. [2] and [3]. The latter should be the case when we consider a space-time symmetric pulse propagating in a slab waveguide in the anomalous dispersion regime. However, in order to sim-

plify further discussion we will neglect the time dependence, and assume the two transverse coordinates to be both spatial.

The solution of Eq. (1.2) can be obtained numerically as, for instance, in Ref. [13], but in the present analysis we shall apply an approximate analytical scheme, the variational technique; cf. [21] and [23]. In this approach, an approximate solution to Eq. (1.2) is obtained by variation within a given set of trial functions. The method has been successful in earlier studies [3,6,10,21], and it is in some cases superior to the paraxial-ray approximation (cf. Refs. [3] and [6]). In the next two sections we will use this analytical approach to examine two separate cases of solutions to Eq. (1.2). Section II is devoted to an investigation of stationary, self-guided beams. In Sec. III we generalize the analysis by considering the dynamic propagation of light beams in saturable media; i.e., we study the combined effects of diffraction and self-focusing with the latter being limited by saturation.

II. STATIONARY SELF-GUIDED BEAMS

When considering stationary solutions of the NLS equation, it is convenient to separate the longitudinal and radial dependencies by assuming a constant phase shift δ along the distance of propagation, viz.,

$$\Psi(r,z)=\Psi(r)\exp\left[-i\frac{\delta\zeta}{2}\right] . \tag{2.1}$$

The dimensionless coordinate ζ is defined as $\zeta=kz$. Inserting this into Eq. (1.2) we obtain the equation that governs the electrical-field envelope in the stationary, saturable case:

$$\frac{1}{\rho}\frac{\partial}{\partial\rho}\left[\rho\frac{\partial\Psi}{\partial\rho}\right]-\delta\Psi+\frac{|\Psi|^2\Psi}{1+\gamma^2|\Psi|^2}=0 , \tag{2.2}$$

where we have also introduced the normalized radial coordinate $\rho=rk$, and the phase delay δ plays the role of an eigenvalue. If the phase shift is used in the normalization of the amplitude and the radial coordinate, we obtain Eq. (2.2) with $\delta=1$, as have been done in the previous numerical investigations [14,21]. It is, however, interesting to examine δ as a function of the nonlinearity. We now reformulate Eq. (2.2) into a variational problem using the Lagrangian

$$L=\rho\left[\frac{\partial\Psi}{\partial\rho}\right]^2+\rho\delta\Psi^2-\frac{\rho}{\gamma^2}\left[\Psi^2-\frac{1}{\gamma^2}\ln(1+\gamma^2\Psi^2)\right] . \tag{2.3}$$

The variational integral can be evaluated explicitly if we choose a trial function for the radial shape $\Psi(\rho)$. This choice is a crucial step in the variational method, because the accuracy of our approximate solutions depends on how well the trial functions approximate the exact solution.

The earlier numerical studies [14,21] of Eq. (2.2) have shown that the shape of the fundamental mode depends strongly upon the degree of saturation. Chen [21] showed that the modal profile can be well approximated with, in turn, hyperbolic, Gaussian, and sine shapes for increasing degree of saturation. In order to analytically reproduce these different shapes, we will choose a super-Gaussian trial function,

$$\Psi(\rho)=A\exp\left[-\frac{1}{2}\left[\frac{\rho}{a}\right]^{2m}\right] , \tag{2.4}$$

where A is the amplitude, a the width, and m the super-Gaussian coefficient. Inserting this trial function into our Lagrangian, and integrating the radial dependence we find

$$\langle L\rangle=\int_0^\infty L\,d\rho=\frac{mA^2}{2}+\left[\delta-\frac{1}{\gamma^2}\right]\frac{a^2A^2}{2}\Gamma\left[1+\frac{1}{m}\right]+\frac{a^2}{2\gamma^4}I(m,K) . \tag{2.5}$$

$\Gamma(x)$ denotes the Gamma function, and I is a function defined by

$$I(m,K)=\int_0^\infty\ln[1+K\exp(-t^m)]dt , \tag{2.6}$$

where $K=(\gamma A)^2$. The constants A, a, and m can now be obtained from the three Euler-Lagrange equations $(\delta\langle L\rangle/\delta A)=(\delta\langle L\rangle/\delta a)=(\delta\langle L\rangle/\delta m)=0$, which give rise to the system

$$(\gamma^2\delta-1)\Gamma\left[1+\frac{1}{m}\right]+\frac{I(m,K)}{K}=0 , \tag{2.7a}$$

$$\frac{m}{2}\left[\frac{\gamma}{a}\right]^2+(\gamma^2\delta-1)\Gamma\left[1+\frac{1}{m}\right]+\frac{\partial I(m,K)}{\partial K}=0 , \tag{2.7b}$$

$$\frac{1}{2}\left[\frac{\gamma}{a}\right]^2-\frac{1}{m^2}(\gamma^2\delta-1)\Gamma'\left[1+\frac{1}{m}\right]+\frac{1}{K}\frac{\partial I(m,K)}{\partial m}=0 . \tag{2.7c}$$

From the above system we can obtain a relation involving only K and m,

$$K\frac{\partial I}{\partial K}=m\frac{\partial I}{\partial m}+I(m,K)\left[1+\frac{\Psi(1+1/m)}{m}\right] , \tag{2.8}$$

where $\Psi(x)$ denotes the logarithm of the Gamma function. Equation (2.8) is a rather complicated, implicit relation between K and m, and it has to be solved numerically. It is, however, possible to find an approximate, empirical relation between K and m, viz.,

$$K(m)\approx 4.48m-3.96+\exp(7.58m-5.42) . \tag{2.9}$$

This relation is plotted in Fig. 1, along with some numerically calculated values of K and m from Eq. (2.8). The agreement is good for $K<500$, and we can now use the relation (2.9) to find the shapes of the stationary fundamental mode in a nonlinear saturable material. Thus we have determined how the modal shape m depends on the parameter K, which is a measure of the degree of saturation. The limit $K=0$ corresponds to the pure nonlinear self-trapped mode. In earlier studies [3,10,21] we have

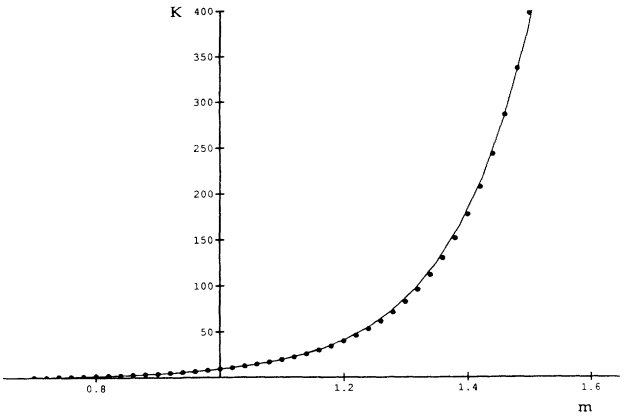

FIG. 1. The relation between the degree of saturation K and the super-Gaussian coefficient m. The dots show numerical computations and the solid line is the empirical relation given by Eq. (2.9).

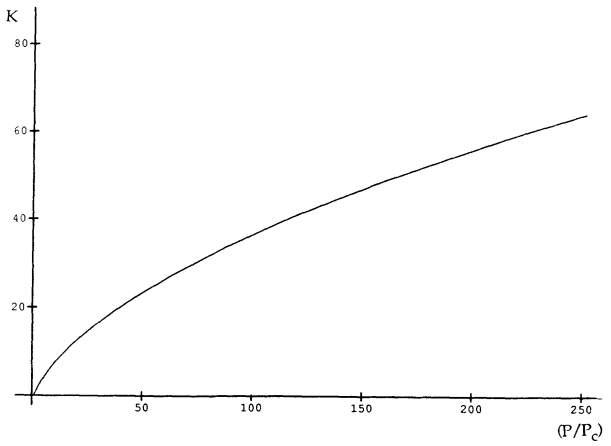

FIG. 2. The parameter K as a function of normalized self-trapped power P/P_c.

seen that the mode profile in this case is well approximated by a hyperbolic secant function. Using the super Gaussian as trial functions in Ref. [10] we have previously shown that the modal shape in the pure nonlinear case in a homogeneous material corresponds to $m=\ln(2)\approx 0.693$, in good agreement with the value obtained by our empirical relation for $K(m)=0$, which yields $m=0.69$.

The phase shift and pulse width can be determined from Eqs. (2.7a) and (2.7b):

$$\delta=\frac{1}{\gamma^2}\left[1-\frac{I(m,K)}{K\Gamma(1+1/m)}\right], \tag{2.10}$$

$$a=\frac{\gamma}{\left[\frac{1}{m}\left[\frac{I}{K}-\frac{\partial I}{\partial K}\right]\right]^{1/2}}. \tag{2.11}$$

Now, we are mainly interested in how these parameters depend on the power of the self-trapped beam, which can be calculated as

$$P\equiv\int_0^\infty 2\pi\rho A^2\exp\left[-\left[\frac{\rho}{a}\right]^{2m}\right]d\rho$$

$$=\frac{K\pi m\Gamma(1+1/m)}{\frac{I}{K}-\frac{\partial I}{\partial K}}. \tag{2.12}$$

Note that the K parameter, the width, the phase shift, and the power are given as functions of the super-Gaussian coefficient m. In the nonsaturable limit $\gamma=0$, corresponding to $m=0.69$, the critical power for self-focusing is $P_c=11.8$ [24]. Self-trapped beams only exist if $P>P_c$, and in Fig. 2, we illustrate the relation between K and (P/P_c). Obviously, the power needed for trapping is higher in the presence of saturation. However, other nonlinear saturable refractive indices can allow stationary beams below P_c (cf. Refs. [11], [14], and [15]).

Figure 3 shows the super-Gaussian coefficient m as a function of beam power. The increase in m becomes very slow for high powers as the refractive index becomes more and more saturated. The normalized phase shift $\delta\gamma^2$ as a function of beam power is plotted in Fig. 4. It increases monotonously with power and has an upper limit equal to unity. Note that the stationary phase shift δ is positive for all powers, indicating that the effective index of the induced waveguide is greater than n_0, previously a point of controversy; cf. [6]. Figure 5 shows the beam width (a/γ) as a function of (P/P_c). The behavior of the width is similar to that given in earlier analytical [16,17] and numerical [11, 14] studies, and it is also very similar to the width for the stationary TE modes, examined in Ref. [20]. We see that self-trapping cannot occur if the pulse width a is too small, or if the relative index difference $(n_{\rm sat}-n_0)/n_0\propto 1/\gamma$ is too low. This fact can qualitatively be obtained from optical ray theory by comparing the diffraction angle for the beam with the angle for total internal reflection at the beam boundary. Narrow beams have larger diffraction angles and will need larger index difference in order to be self-guided. This qualitative discussion has been made earlier in Ref. [8] regarding nonsaturative self-trapping, and in Ref. [21] considering the saturable case. The main difference between the two cases is that in a given saturable media (with a

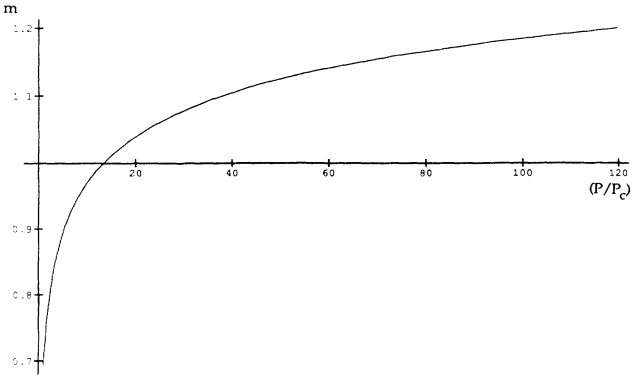

FIG. 3. The shape parameter m vs normalized power. The Gaussian shape $(m=1)$ corresponds to $(P/P_c)=13.46$ and $k=9.24$.

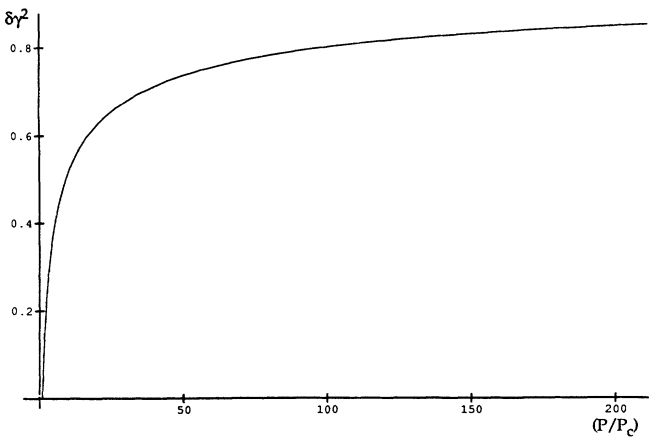

FIG. 4. Nonlinear phase shift δ plotted as a function of power.

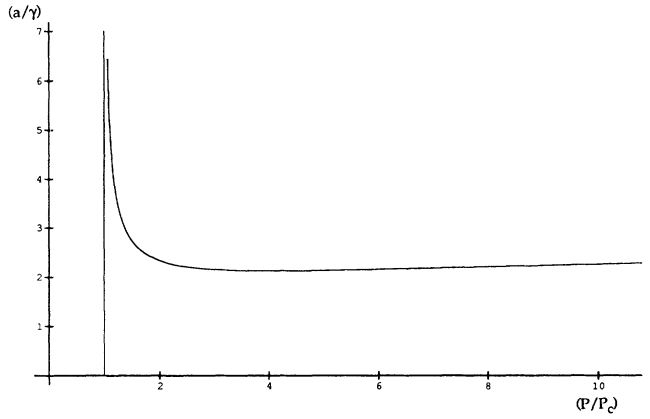

FIG. 5. Dependence of self-trapped beam width on power. The straight line $(P/P_c)=1$ is the low-power asymptote. The minimum beamwidth occurs at $(a/\gamma)=2.12$, and it corresponds to $(P/P_c)=4.1$, $K=3.19$, and $m=0.87$.

given value of γ) there is *both* a minimum beam width $a_{\min}$ and a minimum power P_c below which self-trapping cannot occur, whereas in a nonsaturable media beams of any width can self-trap, provided the amplitude becomes high enough. In this analysis the minimum value of (a/γ) is 2.12; see Fig. 5.

We have collected the self-trapped parameters for a few different degrees of saturation in Table I, along with the exact numerical solutions. The earlier known expressions for a Gaussian trial function [18] can be obtained by putting $m=1$ in Eqs. (2.10) and (2.12), and the results have been added to Table I for comparison. Note that the super-Gaussian trial function does not only provide better approximations, but also additional information about the modal shape behavior through the parameter m. The modal profiles corresponding to the cases of Table I have been plotted in Figs 6(a)–6(c). Our variational model agrees very well with the numerical results, but the agreement starts to deteriorate for high values of K ($K>100$), i.e., the highly saturated case. The super-Gaussian trial function cannot accurately reproduce the modal shape in this limit, since the mode profile effectively consists of two different parts. Near the center, where $\Psi(\rho)$ is large compared to unity, Eq. (2.2) is similar to the equation for the zeroth-order Bessel function. Far from the center, in the region where $\Psi(\rho)$ is comparable to unity, the modal shape starts to decrease exponentially. This is similar to the behavior of the modal shape of the fundamental mode in a step-index fiber. It is difficult to model this kind of modal shape with a super Gaussian, hence the results tend to be less accurate. Therefore, the strongly saturated limit might be better analyzed with the approach suggested by Snyder *et al.* [4], in which the beam is assumed to propagate in a step-index fiber with n_{sat} in the core and n_0 in the cladding. In the region of lower powers, which perhaps could be of greater practical interest, the analytical model presented here should give good approximate solutions of the mode profile.

III. DYNAMIC PROPAGATION

We will now generalize the previous analysis to consider beams whose parameters are allowed to vary with distance of propagation. Approximate analytical solutions to the dynamic form of Eq. (1.2) has earlier been found by using the paraxial-ray approximation [11,12]. More accurate results can be found using the variational scheme [3]. Parts of the following variational analysis have been done earlier, cf. Ref. [18]. However, in the present work we will analyze the results of the variational approach in more detail.

The Lagrangian corresponding to Eq. (1.2) is

$$L=\rho\left|\frac{\partial\Psi}{\partial\rho}\right|^2-\rho i\left[\Psi\frac{\partial\Psi^*}{\partial\zeta}-\Psi^*\frac{\partial\Psi}{\partial\zeta}\right]-\frac{\rho}{\gamma^2}\left[|\Psi|^2-\frac{1}{\gamma^2}\ln(1+\gamma^2|\Psi|^2)\right]. \tag{3.1}$$

TABLE I. Stationary beam parameters compared with numerical solutions for some different amplitudes Ψ_0 ranging from 0.01 to 100. We have chosen $\gamma=1$. The modes are plotted in Figs. 6(a)–6(c).

	Variational approximation						Numerical solution	
	Super Gaussian				Gaussian			
K	m	a	P	δ	P	δ	P	δ
0.01	0.6949	17.27	11.93	0.001 84	12.67	0.002 49	11.79	0.002 05
0.1	0.7035	5.671	12.73	0.018 0	13.69	0.023 9	12.68	0.020 0
1	0.7739	2.430	21.53	0.150	24.29	0.177 5	21.90	0.159 1
10	1.0104	2.375	176.4	0.582	174.5	0.580 1	180.3	0.585 4
100	1.3256	4.680	6330	0.900	4121	0.877 6	5491	0.894 7

Note that $\Psi(\rho,\zeta)$ in this section is a complex-valued function, and that the asterisk denotes complex conjugate. In order to be able to average over the radial coordinate we have to specify the radial shape. Section II showed how the modal shape varies with amplitude in Fig. (3). This dependence is, however, not very strong, and the Gaussian shape, i.e., $m=1$, is a convenient average that will not alter the qualitative behavior of the beam dynamics. The Gaussian will also greatly simplify our calculations. Furthermore, it will make us able to compare the results with the paraxial-ray predictions of Ref. [12]. We will therefore choose a Gaussian trial function:

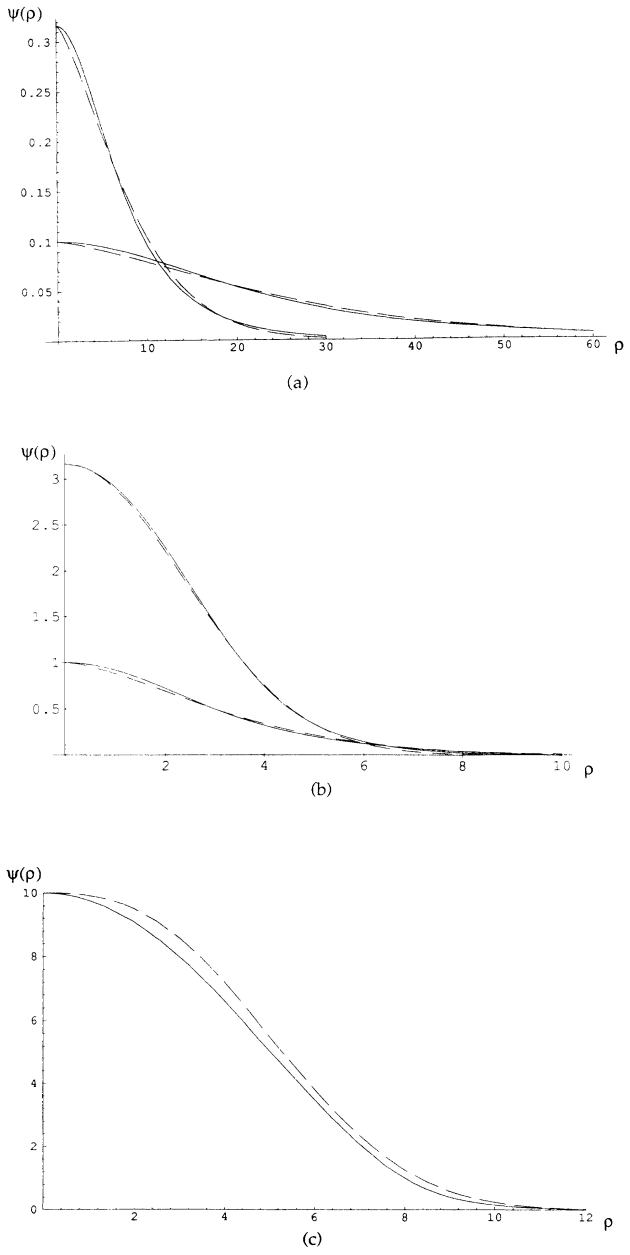

FIG. 6. The modal shapes of the approximate super-Gaussian solutions (dashed) and the numerical solutions (solid) in the cases (a) $K=0.01,0.1$, (b) $K=1,10$, and (c) $K=100$. Note in this example that $K=\Psi_0$.

$$\Psi(\rho,\zeta)=A(\zeta)\exp\left[-\frac{1}{2}\left[\frac{\rho}{a(\zeta)}\right]^2+i\rho^2 b(\zeta)+i\phi(\zeta)\right]. \tag{3.2}$$

There are four real functions of ζ to be determined: the pulse amplitude A, the width a, the phase shift ϕ, and the phase-front curvature b (see [25]). Note that ϕ is defined with a different sign as compared to the phase shift δ of Sec. II. Averaging over the radius will give

$$\langle L\rangle=A^2\left[\frac{1}{2}+a^4\left[2b^2-\frac{\partial b}{\partial\zeta}\right]-a^2\left[\frac{\partial\phi}{\partial\zeta}+\frac{1}{2\gamma^2}\right]\right]+\frac{a^2 l(K)}{2\gamma^4}, \tag{3.3}$$

where $K=[A(\zeta)\gamma]^2$ and the function l is defined by

$$l(x)=\int_0^x\frac{\ln(1+t)}{t}dt. \tag{3.4}$$

Variation with respect to each one of the four unknown functions will give

$$\frac{d}{d\zeta}(A^2a^2)=0, \tag{3.5}$$

$$b(\zeta)=-\frac{1}{2a}\frac{da}{d\zeta}, \tag{3.6}$$

$$\frac{d^2a}{d\zeta^2}=\frac{1}{a^3}\left\{1-\frac{4P}{P_c}\frac{a^4}{a_s^4}\left[1\left[\frac{a_s^2}{a^2}\right]-\ln\left[1+\frac{a_s^2}{a^2}\right]\right]\right\}, \tag{3.7}$$

$$\frac{d\phi}{d\zeta}=\frac{1}{a^2}\left\{1-\frac{4P}{P_c}\frac{a^4}{a_s^4}\left[\frac{1}{2}l\left[\frac{a_s^2}{a^2}\right]+\frac{1}{2}\left[\frac{a_s^2}{a^2}\right]-\ln\left[1+\frac{a_s^2}{a^2}\right]\right]\right\}. \tag{3.8}$$

In the above expressions (P/P_c) denotes $(A_0a_0)^2/4$ (cf. [24]), and $a_s^2=\gamma^2A_0^2a_0^2=Ka_0^2$ where K has the previous definition. The quantity a_s could be interpreted as the width the beam has to have in order to experience saturation effects [12]. We integrate Eq. (3.7) once, and adopt the well-known potential description [12,23] for the width a:

$$\left[\frac{da}{d\zeta}\right]^2+\pi(a)=0, \tag{3.9}$$

where the potential $\pi(a)$ is given by

$$\pi(a)=C+\frac{1}{a^2}+\frac{4P}{P_c}\frac{a^2}{a_s^4}l\left[\frac{a_s^2}{a^2}\right], \tag{3.10}$$

and C is an integration constant. Note that this potential differs considerably from the potential derived with the paraxial-ray method [12]. The constant C is defined by $\pi(a_0)=0$, if we assume the incident beam to be a plane wave. In the subsequent discussion we will use $a_0=1$, which is no restriction, thus $C=-1-4(P/P_c)1(K)/K^2$, and $a_s^2=K$.

A potential function such as Eq. (3.10) yields three qualitatively different behaviors of the width a. If $\pi(a)$ has a second zero a_1 below (above) 1, the width will self-focus (diffract) initially, and oscillate between these two zeros. But since $\pi(a)$ is bounded by $[1-l(K)/K]/\gamma^2-1$ as a approaches infinity, no second zero will exist if the criterion

$$\frac{P}{P_c} < \frac{K^2}{4[K-l(K)]} \tag{3.11}$$

is fulfilled, and the beam will in this case diffract monotonously. Figure 7 gives the potential $\pi(a)$ in these different cases. The criterion for initial self-focusing could be found from the initial sign of the second derivative; cf. Eq. (3.7). Thus, oscillating behavior with initial self-focusing will arise if

$$\frac{P}{P_c} > \frac{K^2}{4[l(K)-\ln(1+K)]} . \tag{3.12}$$

Equations (3.11) and (3.12), and the regimes they bound in the $(P/P_c)-K$ plane are shown in Fig. 8. Note that an equality in Eq. (3.12) would describe the self-trapped solutions studied in Sec. II, and that those stationary solutions are stable since the potential well has a minimum. The fundamental mode may still, however, be unstable to periodic transverse perturbations which is a form of modulational instability (MI). These perturbations can be in either the radial or azimuthal directions. The higher-order modes in a saturable media have recently been found unstable to modulations in the azimuthal directions [26], but the case of the fundamental mode and modulations in the azimuthal direction remains to be investigated. Felber [27] has shown that the exponential growth of a transverse perturbation (filament) will be suppressed in the strongly saturated limit, since the behavior in this limit is nearly linear. Furthermore, if a filament is to be self-guided, it will have to be wider than the minimum beam radius of Fig. 5. Thus we conclude that a sufficiently narrow beam in the strongly saturated limit should not be sensitive to MI. However, a rigorous analysis of the sensitivity to MI for the fundamental beam is beyond the scope of the present analysis.

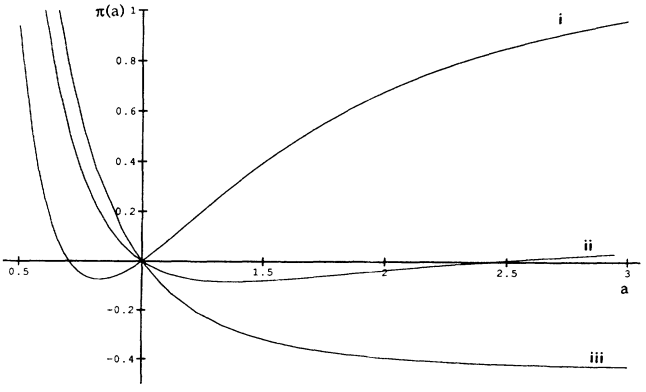

FIG. 7. Potential well $\pi(a)$ in three different cases using $K=2$ and (i) $(P/P_c)=1$, (ii) $(P/P_c)=2$, and (iii) $(P/P_c)=4$.

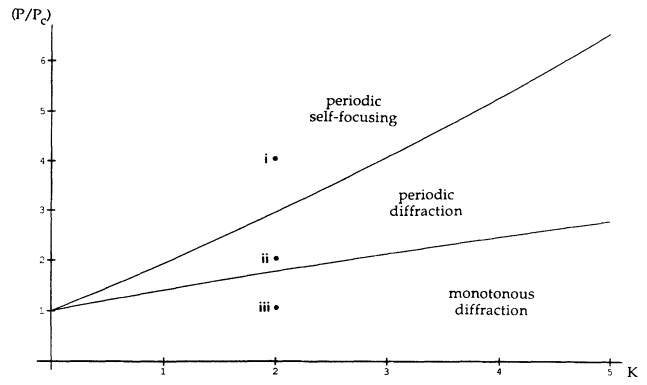

FIG. 8. The different solutions in the (P/P_c)-K plane. The dots correspond to the potentials plotted in Fig. 7.

Considering the second zero a_1, this can be found from the equation $\pi(a_1)=0$, and we can make a contour plot of the different values of a_1 in the parameter plane $[(P/P_c),K]$, as shown in Fig. 9. There are no limits of the contours, implying that any value of a_1 can be reached for any value of K, provided the power becomes high enough. Though Eq. (3.9) cannot be analytically integrated, we can get a quite clear view of the dynamic behavior of $a(\zeta)$ from a phase-plane plot of the width; cf. Fig. 10. Note the increased steepening of the potential well with increased self-focusing, implying faster oscillations. Regarding the period of the oscillations ζ_0, this quantity is a function of (P/P_c) and K, and could be calculated from the expression

$$\zeta_0 = 2\int_{a_1}^{1} \frac{da}{\sqrt{-\pi(a)}} . \tag{3.13}$$

This integral has no simple analytical solutions. It is, however, possible to show that ζ_0 increases with increasing K, and decreases with increasing (P/P_c). The period of oscillation will thus have qualitatively the same dependence on K and (P/P_c) as a_1 have. The minimum value of ζ_0 will occur in the unsaturated nonlinear limit, when

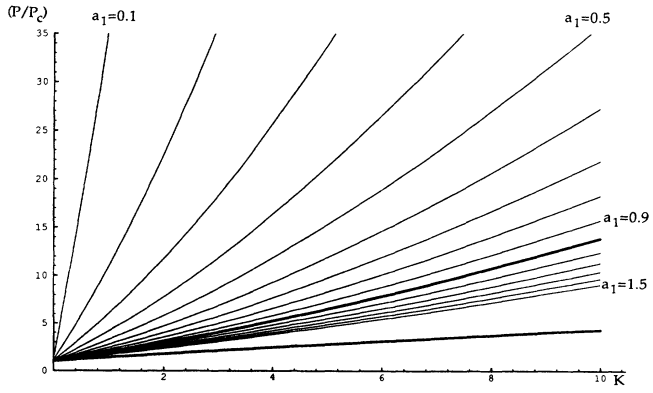

FIG. 9. Maximum ($a_1>1$) and minimum ($a_1<1$) beamwidth in the parameter plane. The contours are plotted from $a_1=0.1$ to 1.5 with spacing 0.1. Thick lines are those of Fig. 8, coinciding with the contours $a_1=1$ and ∞.

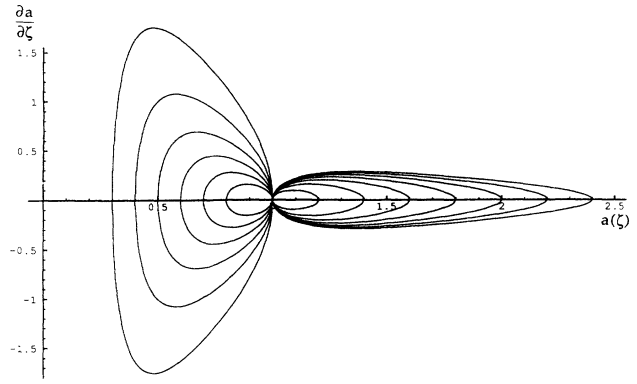

FIG. 10. Phase-plane plots showing the behavior of the width $a(\zeta)$. We have used a fixed value of $K=2$, and have made a_1 take values from 0.3 to 2.4.

$K=0$, and Eq. (3.13) gives the self-focusing distance as $\zeta_0/2=1/\sqrt{(P/P_c-1)}$. This minimum value is also obtained with the paraxial-ray approximation in Ref. [12], although with a lower (by a factor 4) value of P_c.

Finally, we will consider the longitudinal phase shift $\phi(\zeta)$. Equation (3.8) shows that the phase is dependent on ζ through the width $a(\zeta)$. Therefore, if $a(\zeta)$ is oscillating, then ϕ'_ζ will oscillate as well, giving rise to a step-like behavior in ϕ, similar to the behavior in a graded-index fiber [28]. If the right-hand side of Eq. (3.8) is investigated, it will be clear that ϕ'_ζ decreases as the width a grows, and vice versa. The criterion for ϕ'_ζ being initially positive is found from Eq. (3.8) by putting $a=1$:

$$\frac{P}{P_c} < \frac{K^2}{4[\frac{1}{2}I(K)+\frac{1}{2}K-\ln(1+K)]} . \tag{3.14}$$

Above this power the phase derivative will always be negative, i.e., $\phi(\zeta)$ will be monotonously decreasing. Another feature of Eq. (3.8) is that if $P/P_c<\frac{2}{3}$, the phase derivative is always positive, which is due to the propagation approaching the linear behavior (cf. [6] and [28]). Equation (3.14) and the line $P/P_c=\frac{2}{3}$ are shown as thin lines in Fig. 11, and they will divide the parameter plane

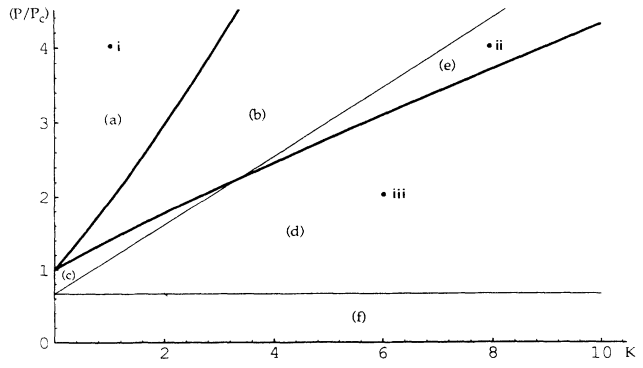

FIG. 11. Taking the phase behavior into account there are six different kinds of propagating beams, corresponding to six domains in the parameter plane. Those have been labeled (a)–(f). The dots (i), (ii), and (iii) correspond to Figs. 12(a)–12(c), respectively.

into several new regimes, which we have denoted (a)–(f). Beams whose parameters lie in the domains above the curve implied by Eq. (3.14) have monotonously decreasing phase shifts, and the width can be either (a) and (b) oscillatory, or (c) monotonously diffracting. If the parameters lie in the areas (d) and (e), the linear behavior is more pronounced; the beam will have initially rising phase shifts, but after a distance of propagation a maximum value is reached, and ϕ starts to decrease. This can occur only once (d), or repeatedly (e). Finally, the low-power regime (f) corresponds to positive, increasing, phase shift of the beam, a behavior that resembles linear

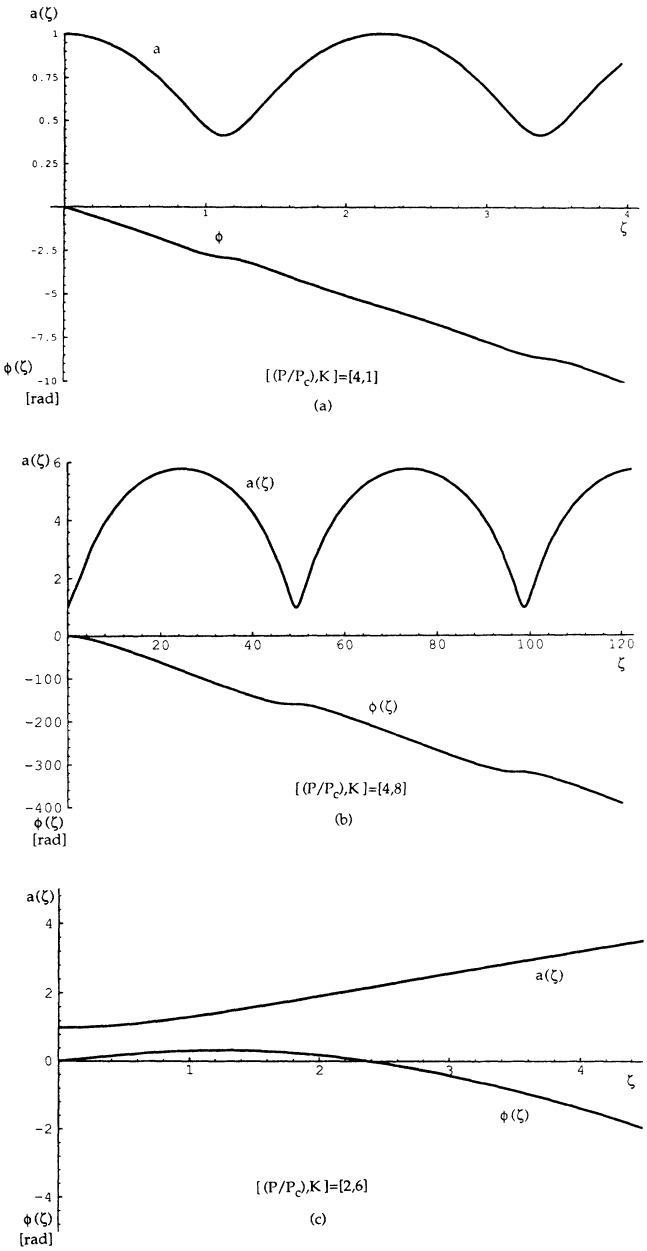

FIG. 12. Numerical solutions of the beamwidth $a(\zeta)$ and phase $\phi(\zeta)$, showing the three different behaviors of the pulse width: (a) oscillatory self-focusing, (b) oscillatory diffracting, and (c) monotonously diffracting.

propagation [6].

We have solved Eqs. (3.7) and (3.8) numerically in a few different cases in order to further clarify the behavior for different combinations of (P/P_c) and K. The solutions are given in Figs. 12(a)–12(c). Figures 12(a) and 12(b) show two oscillatory beams. The phase delay ϕ shows similar behavior in the two cases, with its fastest decrement in the points of maximum width. This is quite contrary to the behavior of the phase in a nonlinear graded-index fiber, in which the phase shift decreases fastest in the points of maximum power [28]. This difference may be qualitatively explained by assuming the nonlinear saturated media to be a linear waveguide. In a linear waveguide, the longitudinal growth rate of the phase ϕ'_ξ, also known as the propagation constant for stationary beams, is inversely proportional to the beam width [29]. The nodes of the beam will experience almost the same waveguide as in the maximum width points, due to the refractive index being saturated. The derivative ϕ'_ξ will thus increase, counteracting the decrement implied by the Kerr effect. This counteracting effect at the nodes will, however, be rather small compared to the overall decrease of the phase. However, the counteraction will be more significant if the Kerr effect is weaker as in the domains (d) and (f). In Fig. 12(c), we see a monotonously diffracting beam with parameters in domain (d). Initially, the saturation is strong enough to overcome the Kerr influence, thus making the phase grow. As the width grows, the Kerr influence will dominate more and more over the saturation, and after some distance of propagation the phase becomes negative. In the case of powers below $2P_c/3$, the Kerr behavior is not strong enough to make the phase decrease, and the linear behavior dominates. Qualitatively speaking, the Kerr influence on the phase shift is limited by the saturation, and powers above $2P_c/3$ will create negative phase shifts first after some distance of propagation. In a pure Kerr media [6], the phase will always be negative when the power is above this limit.

IV. CONCLUSIONS

In conclusion, we have investigated, with an approximate analytical method known to give good accuracy [3,6,23], the properties of beams propagating in nonlinear saturable media. Regarding stationary beams, the variational technique gave very good agreement with numerical calculations. The fact that the modal shape of the fundamental mode differs with the degree of nonlinearity can be understood as due to the different kinds of induced waveguides that arise for different degrees of saturation.

TABLE II. The different shapes of the fundamental mode that may arise in the studied saturable medium, and a few properties of these self-trapped beams.

Degree of saturation	Induced waveguide	Modal shape	Stability
Zero	$\approx\mathrm{sech}^2(r)$	$\approx\mathrm{sech}(r)$	unstable
Medium	parabolic graded index	$\exp(-r^2)$	stable
High	step index	$J_0(r); r<a$ $K_0(r); r>a$	stable

In the absence of saturation we have a waveguide induced only by the Kerr index, and equal to that analyzed by Chiao, Garmire, and Townes [8]. This waveguide is characterized by being unstable against perturbations in amplitude and width. If we take saturation into account there are, roughly speaking, two kinds of waveguides that the self-trapped beam can propagate in: a graded-index guide for low onset of saturation, and a step-index guide in the strongly saturated limit. The graded-index guide will have a Gaussian as fundamental mode, and the step-index mode will be described by two joint Bessel functions [29]. Beams propagating in these kinds of waveguides were shown in Sec. III to be stable against small perturbations in width; see Table II. This has also been shown in other ways in earlier works [4,20]. The sensitivity of these self-trapped beams to modulational instability does, however, remain to be investigated.

The dynamical propagation of a beam in a saturable Kerr-nonlinear media was analyzed using the well-known potential description. The stationary beams were shown stable, and deviations from the stability gave rise to oscillatory behavior. Beams may also diffract monotonously, and these different behaviors correspond to different domains in a parameter plane, spanned by the input power and the degree of saturation. This parameter plane is also very useful when considering the qualitative behavior of both the phase and the amplitude of a wave. It was shown that, in general, a wave in a saturable nonlinear medium can behave in six different ways. Finally, we emphasize that one spatial coordinate may be replaced with time, thus creating a stable, nondiffracting, nondispersing optical pulse: a light bullet.

ACKNOWLEDGMENTS

Useful discussions with Dan Anderson are gratefully acknowledged. This research was partly supported by the Swedish Board for Technical Development.

[1] S. Maneuf, R. Desailly, and C. Froehly, Opt. Commun. **65**, 193 (1988).
[2] Y. Silberberg, Opt. Lett. **15**, 1282 (1990).
[3] M. Desaix, D. Anderson, and M. Lisak, J. Opt. Soc. Am. B **8**, 2082 (1991).
[4] A. W. Snyder, D. J. Mitchell, L. Poladian, and F. Ladouceur, Opt. Lett. **16**, 21 (1991).
[5] Q. Y. Li, C. Pask, and R. A. Sammut, Opt. Lett. **16**, 1083 (1991).
[6] M. Karlsson, D. Anderson, M. Desaix, and M. Lisak, Opt. Lett. **16**, 1373 (1991).
[7] J. S. Aitchison, A. M. Weiner, Y. Silberberg, M. K. Oliver, J. L. Jackel, E. M. Vogel, and P. W. E. Smith, Opt. Lett. **15**, 471 (1990).
[8] R. Y. Chiao, E. Garmire, and C. H. Townes, Phys. Rev. Lett. **13**, 479 (1964).

[9] V. E. Zakharov and A. B. Shabat, Zh. Eksp. Teor. Fiz. **61**, 118 (1971) [Sov. Phys.—JETP **34**, 62 (1972)].
[10] M. Karlsson and D. Anderson, J. Opt. Soc. Am. B **9**, 1558 (1992).
[11] J. H. Marburger, L. Huff, J. D. Reichert, and W. G. Wagner, Phys. Rev. **184**, 255 (1969).
[12] W. G. Wagner, H. A. Haus, and J. H. Marburger, Phys. Rev. **175**, 256 (1968).
[13] J. H. Marburger and E. Dawes, Phys. Rev. Lett. **21**, 556 (1968).
[14] T. K. Gustafson, P. L. Kelly, R. Y. Chiao, and R. G. Brewer, Appl. Phys. Lett. **12**, 165 (1968).
[15] A. H. Piekara, J. S. Moore, and M. S. Feld, Phys. Rev. A **9**, 1403 (1974).
[16] J. F. Lam, B. Lippman, and F. Tappert, Opt. Commun. **15**, 419 (1975).
[17] J. F. Lam, B. Lippman, and F. Tappert, Phys. Fluids **20**, 1176 (1977).
[18] D. Anderson and M. Bonnedal, Phys. Fluids **22**, 105 (1979).
[19] J. Herrmann, J. Opt. Soc. Am. B **8**, 1507 (1991).
[20] Y. Chen, J. Lightwave Technol. **9**, 1208 (1991).
[21] Y. Chen, Opt. Lett. **16**, 4 (1991).
[22] M. S. Sodha, A. K. Ghatak, and V. K. Tripathi, in *Progress in Optics,* edited by E. Wolf (North-Holland, Amsterdam, 1976), Vol. XIII, p. 175.
[23] D. Anderson, Phys. Rev. A **27**, 3135 (1983).
[24] $P_c = 11.83$ is the value of critical power using the super-Gaussian approximation. The exact numerical value is $P_c = 11.70$, cf. Refs. [2], [3], and [10]. In Sec. III $P_c = 4\pi = 12.56$, since the Gaussian is a slightly less accurate trial function, cf. Table I.
[25] If time is assumed to be a transverse coordinate within ρ, as suggested in the introduction, i.e., if $\rho^2 = x^2 + \tau^2$, then the "phase-front curvature" $b\rho^2$ is equal to $bx^2 + b\tau^2$, and the function b has the interpretation as both a spatial curvature and a frequency chirp. The same will be the case for the "width" a, which will be both a spatial width and a temporal duration.
[26] J. M. Soto-Crespo, D. R. Heatley, E. M. Wright, and N. N. Akhmediev, Phys. Rev. A **44**, 636 (1991).
[27] F. S. Felber, Appl. Phys. Lett. **38**, 18 (1981).
[28] M. Karlsson, D. Anderson, and M. Desaix, Opt. Lett. **17**, 22 (1992).
[29] A. Yariv, *Optical Electronics,* 3rd ed. (CBS College, New York, 1985), Chap. 3.